



UNIVERSITY OF LEEDS

This is a repository copy of *Preparation of Iron- and Nitrogen-Codoped Carbon Nanotubes from Waste Plastics Pyrolysis for the Oxygen Reduction Reaction*.

White Rose Research Online URL for this paper:
<http://eprints.whiterose.ac.uk/155394/>

Version: Accepted Version

Article:

Cai, N, Xia, S, Zhang, X et al. (7 more authors) (2020) Preparation of Iron- and Nitrogen-Codoped Carbon Nanotubes from Waste Plastics Pyrolysis for the Oxygen Reduction Reaction. *ChemSusChem*, 13 (5). pp. 938-944. ISSN 1864-5631

<https://doi.org/10.1002/cssc.201903293>

© 2019 Wiley-VCH Verlag GmbH & Co. KGaA, Weinheim. This is the peer reviewed version of the following article: N. Cai, S. Xia, X. Zhang, Z. Meng, P. Bartocci, F. Fantozzi, Y. Chen, H. Chen, P. T. Williams, H. Yang, *ChemSusChem* 2020, 13, 938, which has been published in final form at <https://doi.org/10.1002/cssc.201903293>. This article may be used for non-commercial purposes in accordance with Wiley Terms and Conditions for Use of Self-Archived Versions.

Reuse

Items deposited in White Rose Research Online are protected by copyright, with all rights reserved unless indicated otherwise. They may be downloaded and/or printed for private study, or other acts as permitted by national copyright laws. The publisher or other rights holders may allow further reproduction and re-use of the full text version. This is indicated by the licence information on the White Rose Research Online record for the item.

Takedown

If you consider content in White Rose Research Online to be in breach of UK law, please notify us by emailing eprints@whiterose.ac.uk including the URL of the record and the reason for the withdrawal request.



eprints@whiterose.ac.uk
<https://eprints.whiterose.ac.uk/>

A new method for the preparation of iron and nitrogen co-doped carbon nanotubes from waste plastics pyrolysis for oxygen reduction reaction

Ning Cai,^[b] Sunwen Xia,^[b] Xiong Zhang,^[b] Zihan Meng,^[c] Pietro Bartocci,^{*,[a]} Francesco Fantozzi,^[a] Yingquan Chen,^[b] Hanping Chen,^[b] Paul T. Williams,^[d] Haiping Yang,^{*,[b]}

[a] [a] dr., P., Bartocci, prof. F., Fantozzi
Department of Engineering
University of Perugia
via G. Duranti 67, 06125, Perugia, Italy
E-mail: bartocci@crbnet.it

[b] N., Cai, dr., S., Xia, r. X., Zhang, dr. Y., Chen, prof. H., Chen, prof. H., Yang
State Key Laboratory of Coal Combustion, School of Energy and Power Engineering
Huazhong University of Science and Technology
HUST, Wuhan, 430074, PR China
E-mail: yhp2002@163.com

[c] dr. Z., Meng
State Key Laboratory of Advanced Technology for Materials Synthesis and Processing
Wuhan University of Technology
Wuhan 430070, PR China

[d] prof. P. T., Williams
School of Chemical and Process Engineering
University of Leeds
Leeds, LS2 9JT UK

Supporting information for this article is given via a link at the end of the document.

Abstract: A novel method to prepare iron and nitrogen co-doped carbon nanotubes (Fe-N-CNT) is proposed, based on catalytic pyrolysis of waste plastics. At first carbon nanotubes are produced from pyrolysis of plastic waste over Fe-Al₂O₃; then Fe-CNT and melamine are heated together in inert atmosphere. Different co-pyrolysis temperatures are tested to optimize the electrocatalyst production. Working at a high doping temperature improved the degree of graphite formation and promoted the conversion of nitrogen to a more stable form. Compared with commercial platinum on carbon, the electrocatalyst obtained from pyrolysis at 850 °C, showed remarkable properties, with onset potential of 0.943 V vs RHE and half-wave potential of 0.811 V vs RHE and even better stability and anti-poisoning. In addition, zinc–air batteries tests were also carried out and the optimized catalyst exhibited high maximum power density.

Introduction

Plastic is used in a wide range of consumer and industrial applications because of its versatility and convenience, however, the End of Life (EoL) treatment of the plastic waste, represents a challenge to sustainability^[1]. A recent estimate has shown that the total quantity of plastic waste generated around the world from when plastic manufacturing began to the year 2015 was about 6.3 billion tons; with about 60% of it being thrown away, causing great resources waste and pollution^[2]. Therefore, the

effective transformation and utilization of plastic waste has aroused important attention^[3].

Catalytic pyrolysis is considered to be a possible solution to promote the recycling of plastic waste by converting plastic into carbon nanotubes (CNT)^[4], oil^[5] and high heating value gases^[6]. In particular, carbon nanotubes have attracted increasing concern due to their excellent physical and chemical properties^[7]. Recently, carbon based nanomaterials, like graphene^[8], graphdiyne^[9] and CNT^[10], have been widely used as electrocatalysts. In particular, transition metals doped (Fe, Co, and Ni, etc) and nitrogen doped carbons catalysts (M-N-C) have been considered to be the most promising candidates to replace conventional Pt-based catalysts for the oxygen reduction reaction (ORR) in fuel cells (FCs) or metal-air batteries (MABs)^[11]. Among the different M-N-C catalysts, Fe-N-C catalysts have been extensively studied owing to their excellent catalytic activity^[12]. Both theoretical calculations^[13] and experiments^[14] revealed that nitrogen incorporation and Fe-coordinated carbon species were responsible of great improvements in the ORR activity. Nevertheless, to date, most Fe-N-C catalysts still suffer from unsatisfactory stability or durability in harsh electrolyte solutions due to instability of iron^[15]. More importantly, complicated fabrication processes and expensive chemical reagents also restrict scalable production.

The catalytic pyrolysis of plastics, provides an environmentally friendly and inexpensive strategy to treat a wide range of plastic waste that can be used as carbon precursors^[16]. Carbon nanotubes have a unique structure with particular stability and

excellent electrical conductivity, so that they can be applied as structure reinforcements [17], or for further electrochemical applications, such as for the production of super-capacitors [18].

Although carbon-based materials derived from plastics have recently attracted widespread attention, the application for ORR catalysis are rarely reported. Veksha et al [19] have done some attempts on the electrocatalytic applications and the CNTs electrocatalysts prepared from plastic directly are not as good as commercial Pt/C catalyst. Besides, the use of pyrolysis for nitrogen doped CNT preparation is a brand new and promising technique. In addition, the behavior of micro-structural and physicochemical properties of CNT is still unclear, especially when doped with heteroatoms of nitrogen.

Therefore, the analysis presented in this paper have the following objectives:

- to prepare Fe-CNT from the catalytic pyrolysis of polypropylene, using alumina loaded with iron;
- perform co-pyrolysis of the produced Fe-CNT with melamine to obtain the final Fe-N-CNT catalysts to be used in FCs and MABs to promote ORR. This was done focusing the attention on the optimization of co-pyrolysis final temperature;
- to evaluate the performance of the Fe-N-CNT catalysts with an electrochemical workstation.

Fe-N-CNT850 (obtained at 850°C final co-pyrolysis temperature) exhibited remarkable catalytic activity compared to the 20% Pt/C catalyst and even better stability. This method provides a novel strategy to realize the recycling of waste plastics and large-scale production of carbon nanotubes, and more importantly, it represents a way to prepare low-cost, high-performance nonprecious metal catalysts for ORR.

Results and Discussion

Typical scanning electron microscopy (SEM) and transmission electron microscopy (TEM) images of Fe-N-CNT850 showed that graphitic CNTs were prepared, in which Fe nanoparticles were encapsulated (Figure 1a, b).

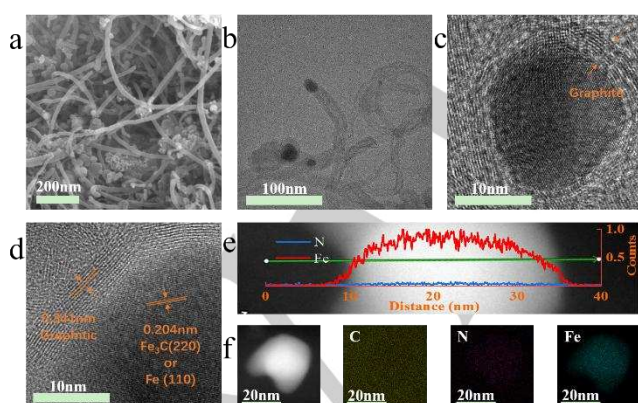


Figure 1. (a) SEM image of Fe-N-CNT850. (b) TEM image of Fe-N-CNT850 with encapsulated Fe nanoparticle. (c) HR-TEM image showing the presence of Fe nanoparticles. (d) HR-TEM image showing the presence of Fe₃C. (e) HAADF-STEM cross-sectional compositional profiles. (f) HAADF-STEM images with elemental mapping of C, N and Fe.

The average outer diameters of carbon nanotubes and the iron nanoparticles in Fe-N-CNT850 are 16.0 nm and 10.8 nm,

respectively (Figure S1). This is due to the small size of the aluminium oxide substrate material (in the order of nanometers), which helped finer iron dispersion for the further catalytic volatiles vapor deposition [20]. The high-resolution TEM (HR-TEM) images revealed that Fe nanoparticles were wrapped with several thin layers (about 10 layers) (Figure 1c, d). Furthermore, the HR-TEM in Figure 1d indicated that the carbon layer spacing out of the nanoparticles was ~0.34 nm, which was corresponding to the graphitic carbon spacing [21]. The lattice fringe inside the nanoparticles was 0.204 nm, this was associated with (220) plane of Fe₃C or (100) plane of Fe [11]. The X-ray diffraction (XRD) spectra in Figure 2a showed that all catalysts have similar positions and numbers of the peaks. The peak at 37.7° appeared after the nitrogen doping process, along with other four peaks at 43.2°, 57.3°, 67.9° and 76.3°, this further confirms the existence of Fe₃C in the synthesized catalysts; Fe₃C has been confirmed to be an efficient catalytic active site in other works [22].

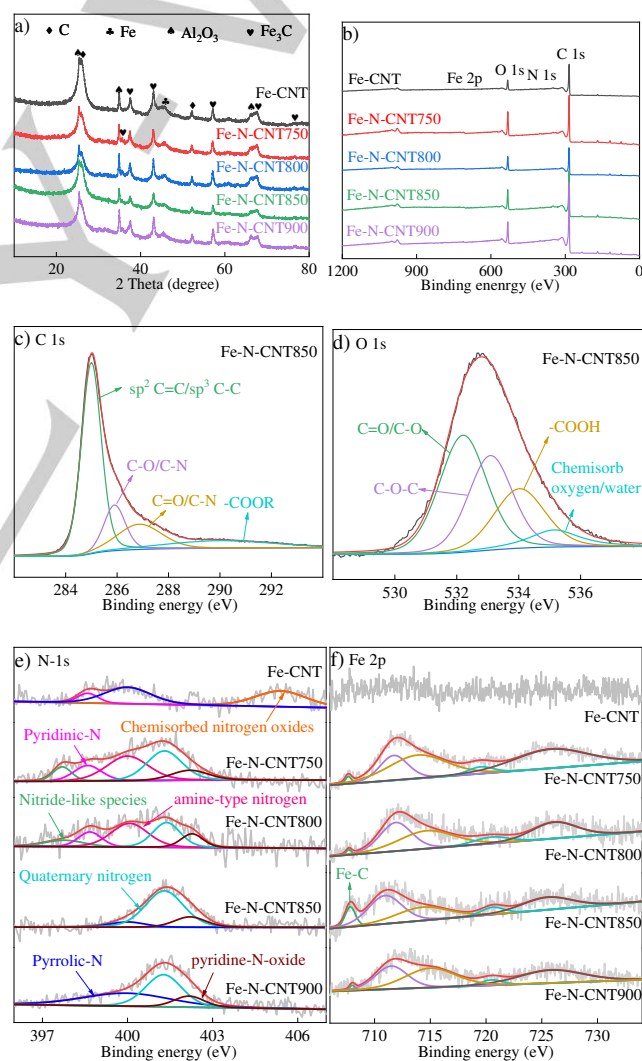


Figure 2. (a) X-ray diffraction of synthesized catalysts. (b) total XPS spectrum of synthesized catalysts. (c) high-resolution XPS spectrum of C 1s for Fe-N-CNT850. (d) high-resolution XPS spectrum of O 1s for Fe-N-CNT850. (e) high-resolution XPS spectrum of N 1s for synthesized catalysts. (f) high-resolution XPS spectrum of Fe 2p for synthesized catalysts.

Simultaneously, the XRD peaks at 26.3° and 45.6° , which are the characteristic peaks of graphite and Fe, were also observed. Furthermore, the line profiles in high-angle annular dark-field scanning TEM (HAADF-STEM) image for a single particle (**Figure 1e**) showed much stronger signal for Fe than N, which indicated that there was a small amount of nitrogen binding to iron after the nitrogen doping process. The TEM-energy-dispersive X-ray (TEM-EDX) revealed that Fe-N-CNT850 was mainly composed of C, encapsulated nanoparticles of Fe and also a small amount of nitrogen (**Figure 1f**).

To further investigate the chemical composition and content of each element in Fe-CNT and Fe-N-CNTs, X-ray photoelectron spectroscopy (XPS) was employed. The full spectrum (**Figure 2b**) of Fe-CNT and Fe-N-CNTs displayed distinctive peaks of C and O, in this case, peaks of N and Fe were apparently not observed because of low content. For further investigation, the high resolution XPS spectra of C, N and Fe are shown in **Figure 2c, d, e** and **f**. The XPS spectrum of C 1s for Fe-N-CNT850 showed that the main sharp peak is located at 285 eV and corresponds to C=C and C-C, which represent the existence of graphitic carbon. The C=C and C-C peaks mainly derive from the ordered graphitization structure of carbon nanotubes which promotes conductivity and electron transport [23]. While the peak at about 285.9 eV is associated with C-O or C-N and the peak at about 286.9 eV corresponds to C=O or C-N, which might correspond to the C-N heterocycles formed during melamine pyrolysis process [24]. The latter peak at ~ 290.2 eV could be ascribed to -COOR, originating from leaching of nitric acid [25] (**Figure 2c**). The XPS spectrum of O 1s for the Fe-N-CNT850 catalyst is shown in **Figure 2d**. The original data could be divided into four peaks, located at 532.2 eV, 533.1 eV, 534.0 eV and 535.2 eV, corresponding to C=O/C-O, C-O-C, -COOH and chemisorbed oxygen/water, respectively. The presence of a large number of oxygen-containing groups facilitates the hydrophilicity of the electrocatalysts and promotes their sufficient contact with the electrolyte, which implies a sufficient contact of reaction media with the active sites [26]. C 1s and O 1s XPS spectra of other samples are shown in **Figure S2** and **S3**. Furthermore, the XPS N 1s spectrum for different catalysts showed several different peaks (**Figure 2e**). The N content of Fe-CNT was 0.34 wt.% and the peak at 405.3 eV was attributed to chemisorbed nitrogen oxides, derived from the nitrate radical functional group introduced by nitric acid leaching. Furthermore, another two peaks at 398.6 eV and 400.0 eV were detected, which were associated with pyridinic-N and pyrrolic-N groups. After the nitrogen doping, the content of N in Fe-N-CNTs increased greatly. Interestingly, existing forms and relative intensities of N for different samples changed distinctly with the increase of doping temperature. This indicates that N-bond configuration is deeply influenced by temperature. The higher the temperature the more stable forms of nitrogen are produced [27]. The XPS N 1s spectra for different nitrogen doping temperatures showed obvious differences, which were reflected in the spectra, where peaks number clearly decreased. When nitrogen doping temperature was 750 °C - 800 °C, nitride-like species occurred for the first time, which could be attributed to the formation of g-CN_x from melamine pyrolysis [28]. Furthermore, compared with Fe-CNT, the content of pyridinic-N in Fe-N-CNT750 and Fe-N-CNT800 increased, which mainly came from the cyclization reactions of O-containing compounds (produced from nitric acid

leaching) reacting with N-containing intermediates derived from melamine pyrolysis (such as NH₃) [29]. However, with the further increase in the doping temperature, the relatively active nitrogen groups, such as nitride-like species and pyridinic-N decreased. When the temperature reached 850 °C, nitride-like species and pyridinic-N disappeared. This might be due to the conversion of some pyridine-N to quaternary-N at high temperature through condensation reactions [29]. Moreover, NH₃ produced from the pyrolysis of the melamine together with the CNTs could also generate some N-containing groups on the surface of Fe-N-CNTs. More importantly, the XPS spectra of Fe 2p for Fe-CNT and Fe-N-CNTs were shown in **Figure 2f**. Compared with Fe-CNT, the relative contents of Fe in Fe-N-CNTs were a little bit higher, which might be ascribed to the damage of the integrity of carbon nanotubes from the nitrogen doping process, and can lead to an increase of iron exposure. The maximum iron content can reach 1.17 wt.% for Fe-N-CNT750, and the relative contents of Fe for other samples are shown in **Table S2**. For Fe-CNT, low Fe content made it difficult to perform further analysis of the corresponding XPS spectrum. Whereas, for Fe-N-CNTs, the Fe 2p XPS spectrum could be divided into several peaks. The peak at 707.8 eV for Fe 2p spectrum of Fe-N-CNT850 corresponds to Fe-C, which was consistent with the TEM and XRD results. In addition, the XPS spectrum of Fe 2p for Fe-N-CNT850 showed much higher peak for Fe-C, derived from melamine catalytic pyrolysis in the presence of Fe.

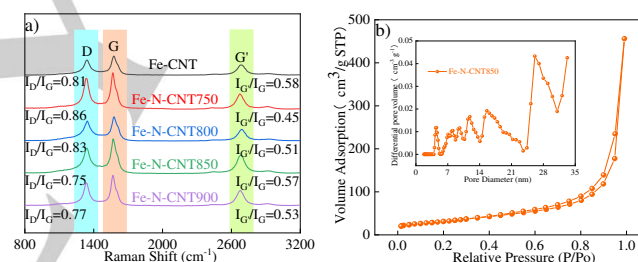


Figure 3. (a) Raman spectra of all samples and (b) N₂ adsorption/desorption isotherms and pore distribution of Fe-N-CNT850.

The graphitic structure of the different samples was further studied by Raman analysis (**Figure 3a**). For all Fe-N-CNT, Raman spectra showed three peaks at about 1340 cm^{-1} (D band), 1580 cm^{-1} (G band), and 2670 cm^{-1} (G' band), corresponding to the sp^3 disordered and defected in graphene, the planar motion of sp^2 -hybridized carbon atoms in the graphite layers and the graphene-like sheets or CNTs, respectively [30]. The number of disordered and defected sites in the carbon structure can be estimated from the relative peak intensity ratio of D to G bands (I_D/I_G) [31]. The I_D/I_G calculated value of Fe-CNT was 0.81. And the I_D/I_G value of Fe-N-CNTs' had a tendency to decrease with the increase of the nitrogen doping temperature. This suggested that higher temperature is favorable for microstructural rearrangement, leading to the decrease in structural defects and the increase in the graphitization degree [10]. In addition, the intensity ratio $I_{G'}/I_G$ could be used to describe the purity of the carbon nanotubes and the higher intensity ratio of $I_{G'}/I_G$ corresponds to higher purity [32]. Compared with Fe-CNT (0.58), the $I_{G'}/I_G$ ratio of Fe-N-CNTs was smaller, this meant that

Fe-N-CNTs had lower purity than Fe-CNT, due to the destructive effect of the nitrogen doping process.

The porous characteristics of all synthesized catalysts were analyzed with the nitrogen adsorption-desorption technique (**Figure 3b and S4**). For example, Fe-N-CNT850 showed a type of IV isotherm and H3 hysteresis loop and the relative pressure of the loop ranged from 0.5 and 1.0, which is one of the main characteristics of mesoporous materials. It also exhibited a specific surface area of $114.4 \text{ m}^2 \text{ g}^{-1}$, a little smaller compared with that of Fe-CNT ($126.1 \text{ m}^2 \text{ g}^{-1}$), due to possible structural damage in the nitrogen doping process. The pore size distribution curve (**Figure 3b inset**) further confirmed the existence of mesoporous structure with pore diameters centered at about 4.4, 10.1, 16.2 and 26.8 nm. This mesoporous structure of the catalyst is very useful in the exposure of active catalytic sites and the diffusion of the electrolyte during the catalytic reactions^[33].

The comparison of CV curves of Fe-CNT, Fe-N-CNTs and 20% Pt/C catalyst showed that reduction peaks for Fe-N-CNTs were more positive than that of Fe-CNT (0.69), suggesting that the oxygen reduction reaction occurred involving oxygen contained in the electrolyte (see **Figure S5**). The linear sweep voltammetry (LSV) curves (**Figure 4a**) exhibited that Fe-N-CNT850 showed higher positive onset potential (the potential at which the ORR starts) of 0.943 V, 137 mV than that of Fe-CNT and that of 20% Pt/C catalyst (only 26 mV negative), respectively. Furthermore, Fe-N-CNT850 showed higher positive half-wave potential of 0.811 V, 156 mV positive compared with that of Fe-CNT and 39 mV negative than that of the 20% Pt/C catalyst, respectively. In short, Fe-N-CNT850 has shown comparable electrocatalytic activities to those of 20% Pt/C catalyst. Fe-N-CNT850 also revealed more positive onset potential and half-wave potential than other synthesized catalysts. The ORR kinetics of Fe-N-CNT850 were evaluated from RDE tests at different rotation speeds, ranging from 800 rpm to 2400 rpm. The limited diffusion current density increased as the rotation rate increased, as a result of the improved mass transport and faster oxygen diffusion to reaction sites (**Figure 4b**). The fitting curves of Koutecky-Levich (K-L) plots presented in **Figure 4c** show almost linear relationships, indicating a first-order reaction kinetics towards the concentration of dissolved O_2 in the solution at different potentials. As can be seen from **Figure 4d**, the numbers of transferred electrons (n) calculated from K-L plots had a similar value, which changed from 3.81 to 3.92 over the potential range of 0.3-0.6 V, which is close to the theoretical value of 4. All above reported the results confirm the remarkable electrocatalytic activities of Fe-N-CNT850. Favorable activities of Fe-N-CNT850 could be ascribed to the co-existence of Fe₃C and N species, especially quaternary-N has good electrical conductivity, which plays an important role for the electrocatalytic process^[34]. Moreover, other catalysts were also evaluated with different rotation rates LSVs and K-L plots, and transfer electron numbers were also simulated (**Figure S6**).

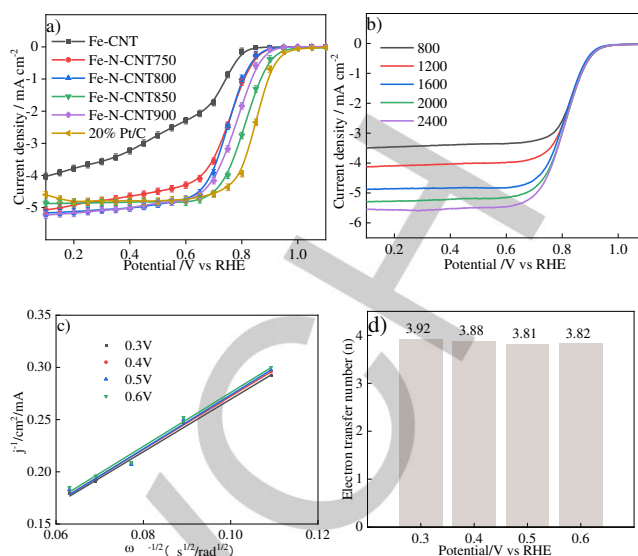


Figure 4. (a) LSV curves of O_2 -saturated solutions at the scan rate of 5 mV s^{-1} with the rotation speed of 1600 rpm for all catalysts. (b) LSV curves of Fe-N-CNT850 at different rotation rates. (c) The corresponding K-L plot of Fe-N-CNT850 at different potentials. (d) The electron transfer number (n) of Fe-N-CNT850 catalyst.

Long-term stability and methanol tolerance of the ORR catalysts are also important and critical indices for the practical application to fuel cells. To evaluate the stability of the synthetic samples, chronoamperometry response was performed in O_2 -saturated 0.1M KOH at 0.6V. For a reference comparison, the stability test of commercial 20% Pt/C was also conducted under the same conditions. There was only a small decrease for Fe-N-CNT850 in the i - t curve after 40000s of uninterrupted working test (In **Figure 5a**), and the current retention rate was higher than that of 20% Pt/C, while Fe-CNT showed about 80% current density of the initial just after the 20000s of testing. Compared with Fe-CNT, the high durability of Fe-N-CNT850 might be due to the flakes of graphitic layers from melamine pyrolysis that may block the openings of the carbon nanotube, which prevented Fe particles, wrapped in CNT, from corrosion and avoiding the dissolution and re-deposition process of metal particles during ORR testing^[35]. In addition, the polarization curves of Fe-N-CNT850 and 20% Pt/C catalyst, obtained before and after 40000 s test are presented in **Figure 5b and 5c**. Compared with the initial result, Fe-N-CNT850 catalyst shows only 9 mV negative in half-wave potential after stability test, which is superior than that of Pt/C catalyst (15 mV). Besides, some characterizations of the Fe-N-CNT850 catalyst after stability test were presented in **Figure S7**. The HAADF-STEM and XPS results shows no obvious changes before and after stability test. All these results further confirm the satisfactory long-term stability of Fe-N-CNT850 catalyst.

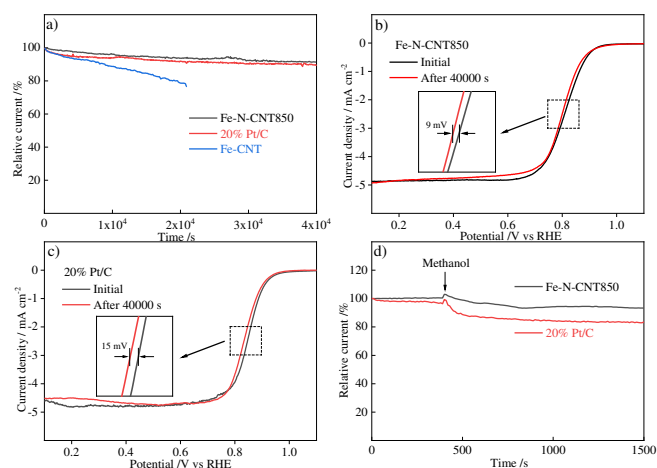


Figure 5. (a) Chronoamperometric responses of Fe-N-CNT850 and 20% Pt/C in O_2 -saturated 0.1 M KOH with a rotation rate of 1600 rpm at 0.6 V. (b) Polarization curves of Fe-N-CNT850 obtained before and after stability test. (c) Polarization curves of Pt/C obtained before and after stability test. (d) Chronoamperometric responses of Fe-N-CNT850 and 20% Pt/C at 0.6 V in O_2 -saturated 0.1 M KOH with and without methanol.

Furthermore, methanol tolerance of Fe-N-CNT850 and Pt/C catalysts was evaluated by chronoamperometry response with and without the existence of methanol. As shown in **Figure 5d**, there was an apparent current drop (decreased more than 15% of the initial current) for the commercial 20% Pt/C catalyst when methanol was introduced into the electrolyte at 400s and the current continued to decay in the followed test. Nevertheless, Fe-N-CNT850 exhibits better methanol tolerance than the 20% Pt/C catalyst and the current of Fe-N-CNT850 decreased slightly after methanol addition and tended to be stable around 800s, which indicated that Fe-N-CNT850 showed higher tolerance to methanol and better resistance to poisoning, compared with the reference Pt/C electrocatalyst. Better stability and methanol tolerance of Fe-N-CNT850 make it possible for it to be a promising candidate for the oxygen reduction reactions.

Further work was undertaken where primary Zn-air batteries were assembled with Fe-N-CNT850 and Pt/C catalyst, and their cell performances were evaluated. Fe-N-CNT850 based Zn-air battery was stable for more than 5000 s of usage at a high open-circuit potential of 1.44 V, which was negligibly lower (0.02 V) than that of the Pt/C based zinc-air battery (1.46 V) (**Figure 6a**). Furthermore, as showed in **Figure 6b**, the Fe-N-CNT850 based zinc-air battery showed a higher peak power density of 120.44 $mW\ cm^{-2}$, while the Pt/C based zinc-air battery exhibited lower peak power density of 98.53 $mW\ cm^{-2}$.

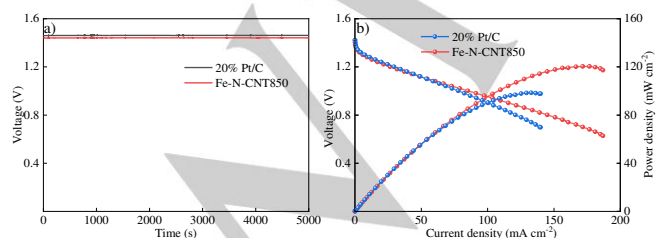


Figure 6. (a) Open circle potentials and (b) Polarization and power density profiles of Zn-air batteries with Cathodic catalyst loaded by Fe-N-CNT850 and 20% Pt/C at $10\ mV\ s^{-1}$.

Conclusion

In conclusion, an easy, controllable and scalable synthesis route was developed to achieve one-dimensional tubular Fe and N co-doped carbon-based materials (Fe-N-CNTs) through catalytic pyrolysis of waste plastics. The optimized Fe-N-CNT850 catalyst displayed better catalytic activity than the pristine Fe-CNT. In particular, compared with Fe-CNT, onset potential and half-wave potential of the Fe-N-CNT850 catalyst shifted 137 mV and 156 mV to the positive, respectively. Fe-N-CNT850 also showed higher limiting-current density than that of Fe-CNT. Furthermore, Fe-N-CNT850 revealed remarkable electrocatalytic activities compared with 20% Pt/C. The significantly enhanced performance of Fe-N-CNT850 was also manifested by better stability and anti-poisoning properties. In addition, a Fe-N-CNT850 based Zn-air battery exhibited a higher power density of 120.44 $mW\ cm^{-2}$ compared to that of 20% Pt/C. The novel catalytic pyrolysis of waste plastics used to prepare electrocatalysts offers a scalable preparation and environmentally-friendly route to rationally designed, practical and highly-active one-dimensional tubular heteroatoms co-doped carbon-based materials, providing an alternative method for developing cheap electrocatalysts for next generation energy related storage technology.

Acknowledgements

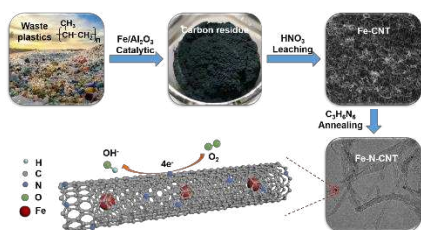
The authors wish to express their sincere thanks for the financial support from the National Key Research and Development Program of China (2018YFC1901204), the National Natural Science Foundation of China (51622604, 51806077 and 51861130362), China Postdoctoral Science Foundation (2018M640696), the Foundation of the State Key Laboratory of Coal Combustion (FSKLCCA1805)). The experiment was also assisted by the Analytical and Testing Center in Huazhong University of Science & Technology (<http://atc.hust.edu.cn>, Wuhan 430074 China).

Keywords: carbon nanotubes • electrochemistry • Fuel cells • Oxygen Reduction Reaction • waste plastics

- Y. Zhao, X. Lv, H. Ni, *Chemosphere* **2018**, 209, 707-720
- a) R. Geyer, J. R. Jambeck, K. L. Law, *Sci. Adv.* **2017**, 3, 1-5; b) J. R. Jambeck, R. Geyer, C. Wilcox, T. R. Siegler, M. Perryman, A. Andrady, R. Narayan, K. Law *Science* **2017**, 347, 768-771; c) M. Bientinesi, L. Petarca, *Waste Manage.* **2009**, 29, 1095-1102
- D. Yao, H. Yang, H. Chen, P. Williams, *Appl. Catal. B: Environ.* **2018**, 227, 477-487
- A. Jonathan, C. Wu, P. Williams, *Appl. Catal. B: Environ.* **2016**, 180, 497-510
- A. Faisal, W. Daud, W. Ashri, *Energy Convers. Manage.* **2014**, 87, 71-85
- A. López, I. de Marco, B. M. Caballero, Laresgoiti, A. Adrados, A. Aranzabal, *Appl. Catal. B: Environ.* **2011**, 104, 211-219
- R. H. Baughman, A. A. Zakhidov, W. A. de Heer, *Science* **2002**, 297-792
- H. Wang, T. Maiyalagan, X. Wang, *ACS Catal.* **2012**, 2, 781-794
- Y. Zhao, J. Wan, H. Yao, L. Zhang, K. Lin, L. Wang, N. Yang, D. Liu, L. Song, J. Zhu, L. Gu, L. Liu, H. Zhao, Y. Li, D. Wang, *Nature chemistry* **2018**, 10, 924-931
- Y. Liu, H. Jiang, Y. Zhu, X. Yang, C. Li, *J. Mater. Chem. A* **2016**, 4, 1694-1701

- [11] W. Jiang, L. Gu, L. Li, Y. Zhang, X. Zhang, L. Zhang, J. Wang, J. Hu, Z. Wei, L. Wan, *J. Am. Chem. Soc.* **2016**, 138, 3570-3578
- [12] a) X. Yang, Y. Zheng, J. Yang, W. Shi, J. Zhong, C. Zhang, X. Zhang, Y. Hong, X. Peng, Z. Zhou, S. Sun, *ACS Catal.* **2016**, 7, 139-145; b) V. Armel, S. Hindocha, F. Salles, S. Bennett, D. Jones, F. Jaouen, *J. Am. Chem. Soc.* **2017**, 139, 453-464; c) J. Tian, A. Morozan, M. T. Sougrati, M. Lefevre, R. Chenitz, J. P. Dodelet, D. Jones, F. Jaouen *Angewandte Chemie* **2013**, 52, 6867-6870
- [13] Y. Zheng, D. Yang, J. Kweun, C. Li, K. Tan, F. Kong, C. Liang, Y. Chabal, Y. Kim, M. Cho, J. Yu, K. Cho, *Nano Energy* **2016**, 30, 443-449
- [14] Z. Zhang, J. Sun, F. Wang, L. Dai, *Angew. Chem., Int. Ed.* **2018**, 57, 9038-9043
- [15] C. Domínguez, F. Pérez-Alonso, J. Gómez de la Fuente, S. A. Al-Thabaiti, S. N. Basahel, A. O. Alyoubi, A. A. Alshehri, M. A. Peña, S. Rojas, *J. Power Sources* **2014**, 271, 87-96
- [16] a) A. Veksha, A. Giannis, W. Oh, V. Chang, G. Lisak, *Fuel Process. Technol.*, 170 (2018), pp. 13-20; b) A. Ahamed, A. Veksha, K. Yin, P. Weerachanchai, A. Giannis, G. Lisak, *J Hazard Mater.*, (2019), pp. 121449
- [17] N. Borsodi, A. Szentés, N. Miskolczi, C. Wu, X. Liu, *J. Anal. Appl. Pyrolysis* **2016**, 120, 304-313
- [18] N. Mishra, S. Shinde, R. Vishwakarma, S. Kadam, M. Sharon, M. Sharon, *AIP Conf. Proc.* **2013**, 228, 1538
- [19] a) J. Moo, A. Veksha, W. Oh, A. Giannis, W. D. C. Udayanga, S. Lin, L. Ge, G. Lisak, *Electrochem. Commun.*, 101 (2019), pp. 11-18; b) A. Veksha, K. Yin, J. Moo, W. Oh, A. Ahamed, W. Chen, P. Weerachanchai, A. Giannis, G. Lisak, *J. Hazard. Mater.*, (2019), pp. 121256
- [20] M. I. Abdul-Wahab, S. D. Jackson, *Applied Catalysis A: General* **2013**, 462-463, 121-128
- [21] X. Zhao, C. M. Hayner, M. C. Kung, H. H. Kung, *Adv. Energy Mater.* **2011**, 1, 1079-1084
- [22] a) C. Zhang, J. Liu, Y. Ye, Z. Aslam, R. Brydson, C. Liang, *ACS Appl. Mater. Interfaces* **2018**, 10, 2423-2429; b) W. Yang, X. Liu, X. Yue, J. Jia, S. Guo, *J. Am. Chem. Soc.* **2015**, 137, 1436-1439; c) Y. Yao, H. Xiao, P. Wang, P. Su, Z. Shao, Q. Yang, *J. Mater. Chem. A* **2014**, 2, 11768-11775
- [23] R. Li, X. Wang, Y. Dong, X. Pan, X. Liu, Z. Zhao, J. Qiu, *Carbon* **2018**, 132, 580-588
- [24] H. Ma, X. Jia, L. Chen, P. Zhu, W. Guo, X. Guo, Y. Wang, S. Li, G. Zou, G. Zhang, P. Bex, *J. Phys.: Condens. Matter* **2002**, 14, 11269-11273
- [25] T. Okpalugo, P. Papakonstantinou, H. Murphy, J. McLaughlin, N. Brown, *Carbon* **2018**, 43, 153-161
- [26] K. Kordek, L. Jiang, K. Fan, Z. Zhu, L. Xu, M. Al-Mamun, Y. Dou, S. Chen, P. Liu, H. Yin, P. Rutkowski, H. Zhao, *Adv. Energy Mater.* **2019**, 9, 1802936
- [27] S. Gao, K. Geng, H. Liu, X. Wei, M. Zhang, P. Wang, J. Wang, *Energy Environ. Sci.* **2015**, 8, 221-229
- [28] L. Yu, L. He, Y. Liu, B. Xu, C. Li, J. Tian, *J. Mater. Sci.* **2007**, 43, 689-695
- [29] W. Chen, K. Li, M. Xia, Y. Chen, H. Yang, Z. Chen, X. Chen, H. Chen, *Bioresour Technol* **2018**, 263, 350-357
- [30] M. S. Dresselhaus, A. Jorio, M. Hofmann, G. Dresselhaus, R. Saito, *Nano Lett* **2010**, 10, 751-758
- [31] X. Ling, Y. Wei, L. Zou, S. Xu, *Applied Surface Science* **2013**, 276, 159-166
- [32] R. A. DiLeo, B. J. Landi, R. P. Raffaele, *Journal of Applied Physics* **2007**, 101, 064307
- [33] Y. Hou, Z. Zhao, Z. Yu, S. Zhang, S. Li, J. Yang, H. Zhang, C. Liu, Z. Wang, *J. Qiu, Chemistry* **2018**, 24, 2681-2686
- [34] H. Yang, J. Miao, S. Hung, J. Chen, H. Tao, X. Wang, L. Zhang, R. Chen, J. Gao, H. Chen, L. Dai, B. Liu, *Sci. Adv.*, **2016**, 2, 1-11
- [35] Y. Wang, L. Wang, M. Tong, X. Zhao, Y. Gao, H. Fu, *Nanoscale* **2018**, 10, 4311-4319

Entry for the Table of Contents



Fe-CNT is produced from the catalytic pyrolysis of polypropylene, using alumina loaded with iron. Co-pyrolysis of Fe-CNT with melamine obtains the final Fe-N-CNT catalysts. ORR activity of Fe-N-CNTs is comparable to commercial 20 % Pt/C catalyst.

@PietroBartocci